

Detection of the Hydrophobic Surface Force in Foam Films by Measurements of the Critical Thickness of the Film Rupture

J. K. Angarska,[†] B. S. Dimitrova,[†] K. D. Danov,[‡] P. A. Kralchevsky,^{*,‡}
K. P. Ananthapadmanabhan,[§] and A. Lips[§]

Department of General Chemistry, University of Shumen, 9712 Shumen, Bulgaria,
Laboratory of Chemical Physics & Engineering, Faculty of Chemistry,
University of Sofia, 1164 Sofia, Bulgaria, and Unilever Research U.S.,
45 River Road, Edgewater, New Jersey 07020

Received September 18, 2003. In Final Form: December 12, 2003

At sufficiently high electrolyte concentrations (at suppressed electrostatic repulsion), the free foam films thin gradually, until reaching a certain critical thickness, and then they break. The value of this critical thickness is sensitive to the magnitude of the attractive surface forces acting in the film. We experimentally investigated the rupture of the films formed from aqueous solutions of sodium dodecyl sulfate (SDS) in the presence of 0.3 M NaCl added. The theoretical fits of the data indicate that the van der Waals interaction, alone, is insufficient to explain the measured critical thickness, especially for the lower SDS concentrations. If the difference is attributed to the hydrophobic attraction, then a very good agreement between the theory and experiment is achieved. From the best fit, we determine that the decay length of the hydrophobic force is about 15.8 nm, which coincides with the value obtained by other authors for hydrophobized mica surfaces. The strength of the hydrophobic interaction increases with the decrease of the SDS concentration, which can be explained with the fact that between the adsorbed surfactant molecules greater areas of bare hydrophobic air–water interface are uncovered. In the investigated concentration range, the strength of the hydrophobic force is found to be inversely proportional to the surface density of the adsorbed ions.

1. Introduction

If the thickness of a free liquid film gradually decreases owing to the drainage of liquid, the film typically breaks when it reaches a sufficiently small thickness, called the *critical thickness*, unless some repulsive surface forces are able to provide stabilization. The mechanism of breakage (in the absence of repulsive forces) was proposed by de Vries¹ and developed in subsequent studies.^{2–8} According to this mechanism, the film ruptures as a result of the growth of the capillary waves at the film surfaces (Figure 1) promoted by the attractive surface forces (i.e., the van der Waals forces), which are operative in the film. In fact, thermally excited fluctuation capillary waves are always present on the film surfaces. With the decrease of the average film thickness h , the attractive surface force enhances the amplitude of some modes of the fluctuation waves. At the critical thickness h_{cr} , the two film surfaces locally touch each other because of the surface corrugations, and then the film breaks.⁶ A recent version of this

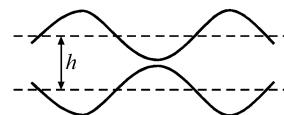


Figure 1. According to the capillary-wave mechanism, the rupture of a free liquid film is a result of the growth of the capillary waves promoted by the attractive surface forces (van der Waals, hydrophobic, etc.); h is the thickness of the nonperturbed film.

capillary-wave model, which takes into account all of the essential physicochemical and hydrodynamic factors, shows an excellent agreement with the experiment.^{7,8}

An example is shown in Figure 2 where the data by Manev et al.⁹ for the critical thickness of foam films are fitted by means of the detailed capillary-wave model.⁷ The data are obtained for films formed in a capillary cell¹⁰ (inner radius $R_c = 1.79$ mm) from 0.43 mM aqueous solutions of sodium dodecyl sulfate (SDS) with 0.25 M NaCl added. The main role of the surfactant, SDS, is to render the film surfaces tangentially immobile, which defines the hydrodynamic regime of film drainage (this is important for the quantitative interpretation of the data). At 0.25 M NaCl, the repulsive electrostatic (double layer) surface force is suppressed; it is completely negligible for the experimental range of the film thickness, $h > 25$ nm (see Figure 2). For this reason, only the attractive van der Waals surface force is operative in these films. Then, all of the parameters of the theoretical model are known, and the theoretical curve in Figure 2 has been drawn *without* using any adjustable parameters.⁷ The effect of the electromagnetic retardation on the dispersion inter-

* Author to whom correspondence should be addressed at 1 J. Bourchier Ave., 1164 Sofia, Bulgaria. Phone: (+359) 2-962 5310. Fax: (+359) 2-962 5643. E-mail: pk@lcpe.uni-sofia.bg.

[†] University of Shumen.

[‡] University of Sofia.

[§] Unilever Research U.S.

(1) de Vries, A. *Recl. Trav. Chim. Pays-Bas* **1958**, *77*, 383. de Vries, A. *Rubber Chem. Technol.* **1958**, *31*, 1142.

(2) Scheludko, A. *Proc. K. Ned. Akad. Wet., Ser. B* **1962**, *65*, 87.

(3) Vrij, A. *Discuss. Faraday Soc.* **1966**, *42*, 23.

(4) Ivanov, I. B.; Radoev, B.; Manev, E.; Scheludko, A. *Trans. Faraday Soc.* **1970**, *66*, 1262.

(5) Ivanov, I. B.; Dimitrov, D. S. *Colloid Polym. Sci.* **1974**, *252*, 982.

(6) Ivanov, I. B. *Pure Appl. Chem.* **1980**, *52*, 1241.

(7) Danov, K. D.; Kralchevsky, P. A.; Ivanov, I. B. In *Encyclopedic Handbook of Emulsion Technology*; Sjöblom, J., Ed.; Marcel Dekker: New York, 2001; Chapter 26, pp 621–659.

(8) Valkovska, D. S.; Danov, K. D.; Ivanov, I. B. *Adv. Colloid Interface Sci.* **2002**, *96*, 101.

(9) Manev, E. D.; Sazdanova, S. V.; Wasan, D. T. *J. Colloid Interface Sci.* **1984**, *97*, 591.

(10) Scheludko, A.; Exerowa, D. *Kolloid-Z.* **1959**, *165*, 148.

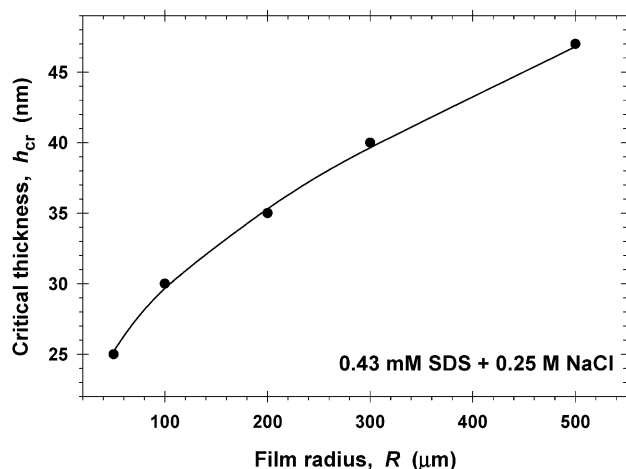


Figure 2. Critical thickness h_{cr} versus radius R of foam films formed from an aqueous solution of 0.43 mM SDS + 0.25 M NaCl, with a comparison between the experimental points, measured by Manev et al.,⁹ and the theory^{7,8} (the solid line; no adjustable parameters).

action has been taken into account; otherwise, the theoretical curve does not comply with the experimental points. The achieved agreement between the theory and experiment is excellent (Figure 2). Similar fits for the critical thickness of foam and emulsion films can be found in ref 8.

The above results mean that in the investigated foam films there is no effect of the hydrophobic surface force (the latter would bring some extra attraction, in addition to the van der Waals force). The absence of hydrophobic attraction is not surprising because, at the experimental surfactant and salt concentrations (0.43 mM SDS and 0.25 M NaCl), the SDS adsorption layer at the air–water interface is closely packed, and the film surfaces are hydrophilic. However, if the concentration of SDS is reduced, the surface density of SDS will diminish, and the zones of the bare air–water interface will appear between the adsorbed surfactant molecules. Because the air phase is regarded as hydrophobic,^{11–13} this could lead to the appearance of a hydrophobic attraction between the film surfaces, which, in its own turn, will increase the critical thickness of the film rupture. Because the available theory of critical thickness works excellently (Figure 2), such an effect could be detected as a deviation of the experimental data from the theoretical prediction based on the action of the van der Waals forces alone. This is the basic idea of the present paper.

The accumulated experimental and theoretical results imply that there are at least two kinds of hydrophobic surface forces of nonelectrostatic physical origin: (i) due to the gaseous capillary bridges (cavitation) between the hydrophobic surfaces^{14–16} and (ii) due to hydrogen-bond-propagated ordering of water molecules in the vicinity of such surfaces,^{17–19} a review was recently published by

Christenson and Claesson.²⁰ In the former case, the formation of the gaseous capillary bridges leads to jumps in the experimental force–distance dependence, and, moreover, the strength of the interaction increases with the concentration of gas dissolved in water.^{21–27} For the second kind of hydrophobic force, the attraction is monotonic and decays exponentially at long distances, with a decay length of about 15.8 nm.^{17,28} In principle, the two kinds of hydrophobic surface forces could act simultaneously, and it is not easy to differentiate their effects.

Back to the breakage of foam films, we may expect that only the hydrophobic surface force of the second kind (that due to molecular ordering) is operative. Indeed, if a nanobubble, like those detected on solid surfaces,^{27,29} is present close to the air–water interface, it will immediately coalesce with the adjacent large air phase. There are numerous data proving the existence of the ordering of water molecules in the vicinity of a hydrophobic boundary, which can be either a macroscopic interface or a separate hydrocarbon molecule.^{18,30} For example, it is known that the standard free energy of adsorption of a surfactant at the air–water interface

$$\Delta G_{ad}^0 = \Delta H_{ad}^0 - T\Delta S_{ad}^0 \quad (1)$$

is dominated by the entropy contribution $T\Delta S_{ad}^0$ rather than by the adsorption enthalpy ΔH_{ad}^0 .^{31–33} For both ionic and nonionic surfactants, the typical values are $|\Delta H_{ad}^0| = 1–7$ kJ/mol, whereas $T\Delta S_{ad}^0 = 23–37$ kJ/mol (see, e.g., refs 32 and 33 and Table 2 in ref 34). In other words, the transfer of the surfactant hydrocarbon tail from an aqueous into an airy environment is accompanied by a considerable increase of entropy, which can be attributed to the disappearance of the shells of the ordered water molecules around each hydrocarbon chain.

Furthermore, if we have a hydrophobic interface, rather than a separate hydrocarbon chain, the ordering of the subsurface water molecules will propagate into the bulk of the aqueous phase.^{17,18} Such ordering is entropically unfavorable. When two hydrophobic surfaces approach each other, the entropically disfavored water is ejected into the bulk, thereby reducing the total free energy of the system. The resulting attraction can in principle explain the hydrophobic surface force of the second kind.^{17,18}

(19) Paunov, V. N.; Sandler, S. I.; Kaler, E. W. *Langmuir* **2001**, *17*, 4126.

(20) Christenson, H. K.; Claesson, P. M. *Adv. Colloid Interface Sci.* **2001**, *91*, 391.

(21) Rabinovich, Y. I.; Yoon, R.-H. *Colloids Surf., A* **1994**, *93*, 263.

(22) Meagher, L.; Craig, V. S. J. *Langmuir* **1994**, *10*, 2736.

(23) Craig, V. S. J.; Ninham, B. W.; Pashley, R. M. *Langmuir* **1999**, *15*, 1562.

(24) Yakubov, G. E.; Butt, H.-J.; Vinogradova, O. *J. Phys. Chem. B* **2000**, *104*, 3407.

(25) Attard, P. *Langmuir* **2000**, *16*, 4455.

(26) Ederth, T.; Tamada, K.; Claesson, P. M.; Valiokas, R.; Colorado, R.; Graupe, M.; Shmakova, O. E.; Lee, T. R. *J. Colloid Interface Sci.* **2001**, *235*, 391.

(27) Tyrrell, J. W. G.; Attard, P. *Langmuir* **2002**, *18*, 160.

(28) Claesson, P. M.; Christenson, H. K. *J. Phys. Chem.* **1988**, *92*, 1650.

(29) Ishida, N.; Inoue, T.; Miyahara, M.; Higashitani, K. *Langmuir* **2000**, *16*, 6377.

(30) Tanford, C. *The Hydrophobic Effect: Formation of Micelles and Biological Membranes*; Wiley: New York, 1973.

(31) Clint, J. H.; Corkill, J. M.; Goodman, J. F.; Tate, J. R. *J. Colloid Interface Sci.* **1968**, *28*, 522.

(32) Rosen, M. J.; Cohen, A. W.; Dahanayake, M.; Hua, X.-Y. *J. Phys. Chem.* **1982**, *86*, 541.

(33) Dahanayake, M.; Cohen, A. W.; Rosen, M. J. *J. Phys. Chem.* **1986**, *90*, 2413.

(34) Durbut, P. Surface Activity. In *Handbook of Detergents, Part A: Properties*; Broze, G., Ed.; Marcel Dekker: New York, 1999; Chapter 3.

(11) Ducker, W. A.; Xu, Z.; Israelachvili, J. N. *Langmuir* **1994**, *10*, 3279.

(12) Yoon, R.-H.; Pazhianur, R. *Colloids Surf., A* **1998**, *144*, 59.

(13) Ralson, J.; Fornasiero, D.; Mishchuk, N. *Colloids Surf., A* **2001**, *192*, 39.

(14) Yushchenko, V. S.; Yaminsky, V. V.; Shchukin, E. D. *J. Colloid Interface Sci.* **1983**, *96*, 307.

(15) Pashley, R. M.; McGuiggan, P. M.; Ninham, B. W.; Evans, D. F. *Science* **1985**, *229*, 1088.

(16) Christenson, H. K.; Claesson, P. M. *Science* **1988**, *239*, 390.

(17) Eriksson, J. C.; Ljunggren, S.; Claesson, P. M. *J. Chem. Soc., Faraday Trans. 2* **1989**, *85*, 163.

(18) Israelachvili, J. N. *Intermolecular and Surface Forces*; Academic Press: London, 1992.

Two attempts^{35,36} have been made to establish the existence of the hydrophobic interaction in equilibrium foam films stabilized by ionic surfactants. However, in this case, the hypothetical hydrophobic force would appear on the background of the powerful electrostatic double-layer repulsion. In such a case, there is always a doubt that an error (overestimation) of the indirectly determined surface electric potential can lead to the calculation of a compensating apparent hydrophobic attraction. For that reason, we decided to search for the hydrophobic attraction in the case when the electrostatic repulsion is suppressed, which is at high salt concentrations. Correspondingly, in our experiments, we measure the critical thickness of the film rupture, rather than the equilibrium film thickness. The latter does not exist if the electrostatic repulsion is suppressed.

Thus, our aim in the present paper is to obtain and interpret data for the critical thickness of breakage of the thinning foam films at low SDS concentrations, at which the existence of the hydrophobic surface force is expected. To interpret the data, the total disjoining pressure Π , operative in the films, will be expressed as a sum of the van der Waals and hydrophobic contributions

$$\Pi(h) = \Pi_{\text{vw}}(h) + \Pi_{\text{hb}}(h) \quad (2)$$

(the electrostatic component of disjoining pressure being negligible). The dependence $\Pi_{\text{vw}}(h)$, accounting for the electromagnetic retardation effect, is specified in section 3.3 below, while for $\Pi_{\text{hb}}(h)$, we use the expression derived by Eriksson et al.¹⁷

$$\Pi_{\text{hb}}(h) = -\frac{B}{4\pi\lambda} \frac{1}{\sinh^2(h/2\lambda)} \quad (3)$$

The parameters B and λ characterize respectively the strength of the hydrophobic interaction and its decay length. According to ref 17, B should increase with the degree of hydrophobicity of the surfaces, whereas the decay length λ should be the same for all of the hydrophobic surfaces under identical solution conditions. Equation 3 was successfully applied by Paunov et al.¹⁹ to interpret the emulsification data.

The paper is organized as follows: Section 2 describes the experimental procedure and results. Section 3 gives an outline of the theory used for the critical thickness of the film rupture h_{cr} and the computational procedure. In section 4, which is devoted to the comparison of the theory and experiment, the values of B and λ are presented and discussed. Let us mention in advance that the results really indicate the existence of an additional attraction in foam films at very low concentrations of SDS and that the determined decay length λ of this attraction complies very well with the λ values obtained by Eriksson et al.¹⁷ for solid hydrophobic surfaces.

2. Experimental Section

2.1. Experimental Method. We formed horizontal foam films from fresh solutions of SDS at concentrations of 0.5, 1, and 10 μM ($1 \mu\text{M} = 1 \times 10^{-6} \text{ mol/dm}^3$) at two fixed concentrations of NaCl (0.1 and 0.3 M). The surfactant solutions were prepared from fresh stock solutions of concentrations of 1×10^{-3} and 5×10^{-3} M SDS to reduce the possible effect of hydrolysis of SDS to dodecanol.

The films were formed in a Scheludko capillary cell¹⁰ of inner radius $R_c = 2.2 \text{ mm}$ (Figure 3). By adjustment of the capillary

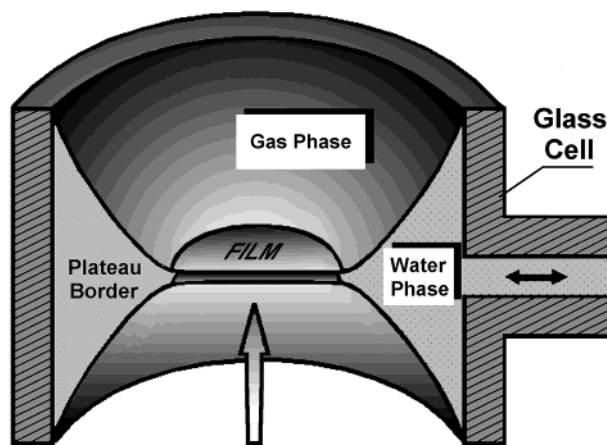


Figure 3. Sketch of the experimental capillary cell.¹⁰ First, the cylindrical glass cell is filled with the working liquid (i.e., water solution). Next, a portion of the liquid is sucked out from the cell through the orifice in the glass wall. Thus, in the central part of the cell, a liquid film is formed, which is encircled by a Plateau border. The arrow denotes the direction of the illumination and microscope observation.

pressure, it was possible to control the film radius R . We carried out experiments at five different fixed radii: 62, 93, 116, 132, and 155 μm . The latter values were convenient because they corresponded to integer numbers of the microscope-scale divisions. From each solution and for each value of R , we formed 15 films to check the reproducibility and accuracy of the measured film thickness h . The optical microscopic observations and measurements of h were carried out in reflected monochromatic light of wavelength $\lambda_0 = 551 \text{ nm}$. In particular, h was determined from the registered intensity I of the light reflected from the film by means of the formula^{37,38}

$$h = \left(\frac{\lambda_0}{2\pi n} \right) \arcsin \left\{ \frac{\Delta}{1 + [4Q/(1-Q)^2](1-\Delta)} \right\} \quad (4)$$

where $\Delta = (I - I_{\text{min}})/(I_{\text{max}} - I_{\text{min}})$, h is calculated assuming a homogeneous refractive index equal to the bulk solution value ($n = 1.33$), $Q = (n-1)^2/(n+1)^2$, I is the instantaneous value of the reflected intensity, and I_{max} and I_{min} refer to the last interference maximum and minimum values. The intensity I was registered by means of a photomultiplier, whose electric signal was recorded as a function of time.

The capillary pressure P_c of the meniscus around the film (which enters the theoretical expressions; see section 3.2) is estimated by using the equation³⁹

$$P_c = \frac{2\sigma R_c}{R_c^2 - R^2} \quad (5)$$

where σ is the surface tension of the solution. For the solutions containing 0.3 M NaCl, we measured $\sigma = 71.3, 70.8,$ and 65.4 mN/m for 0.5, 1, and 10 μM SDS (Wilhelmy plate technique), respectively; the temperature was 25 $^\circ\text{C}$.

2.2. Experimental Observations. The investigated films behaved in the following way. After the initial dynamic stages of the film thinning, almost plane-parallel films formed, whose thickness was gradually decreased. They looked dark gray in the reflected light (Figure 4a). We observed three alternative scenarios of the film rupture:

(a) The dark gray film (of thickness above 20 nm) ruptures as it slowly thins (without formation of black spots).

(b) Black spots (corresponding to the secondary film or Newton black film) appear within the thinning dark gray film, and the latter ruptures immediately after the spots appear.

(37) Scheludko, A.; Platikanov, D. *Kolloid-Z.* **1961**, *175*, 150.

(38) Bergeron, V.; Radke, C. J. *Langmuir* **1992**, *8*, 3020.

(39) Toshev, B. V.; Ivanov, I. B. *Ann. Univ. Sofia Fac. Chem.* **1970**, *71*, 65, 329.

(35) Tchaliowska, S.; Manev, E. D.; Radoev, B. P.; Eriksson, J. C.; Claesson, P. M. *J. Colloid Interface Sci.* **1994**, *168*, 190.

(36) Yoon, R.-H.; Aksoy, B. S. *J. Colloid Interface Sci.* **1999**, *211*, 1.

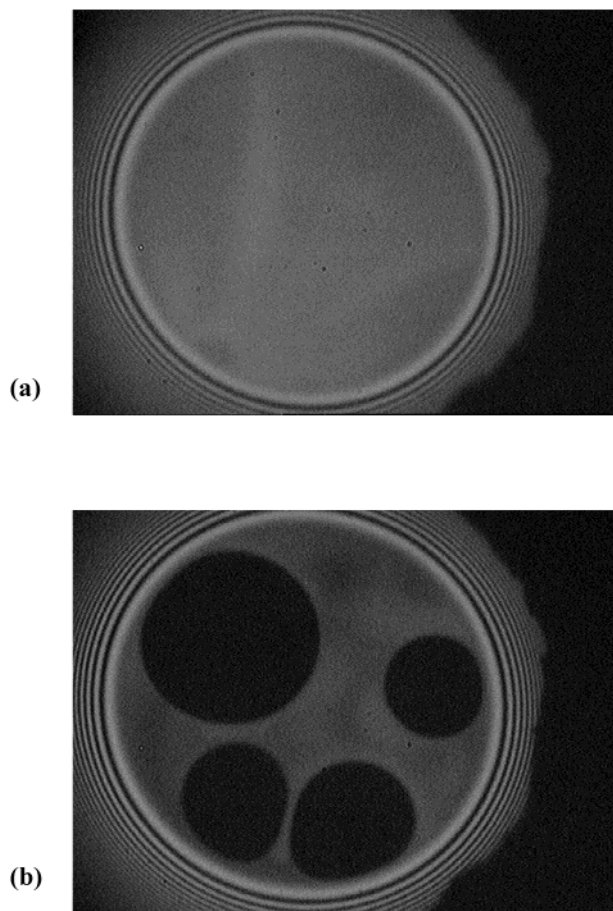


Figure 4. Photos of the thinning films of radius $R = 155 \mu\text{m}$ formed from a solution of $10 \mu\text{M}$ SDS. (a) At 0.3 M NaCl, the film looks dark gray in the reflected light just before it ruptures. (b) At 0.1 M NaCl, the formation of black spots, corresponding to a secondary film, is seen. In both photos, the film is encircled by Newton interference rings located in the Plateau border.

(c) The film safely reaches an equilibrium state of primary (common black) film of thickness $10\text{--}14 \text{ nm}$, in which, after some time, the black spots appear (Figure 4b) and the film ruptures.

(For information about the physical reason for the existence of primary and secondary films, see e.g., ref 40.) At concentrations of 0.5 and $1 \mu\text{M}$ SDS + 0.3 M NaCl, all of the films followed scenario a. At concentrations of $10 \mu\text{M}$ SDS + 0.3 M NaCl, a part of the films followed scenario a, whereas the rest of the films followed scenario b. At concentrations of $10 \mu\text{M}$ SDS + 0.1 M NaCl, we observed a parallel realization of the three alternative scenarios a, b, or c with different films.

The occurrence of scenario c with films containing 0.1 M NaCl means that some residual electrostatic repulsion (barrier) is present, which makes possible the existence of the equilibrium primary films, despite the relatively high NaCl concentration. For this reason, in the further experiments and theoretical interpretation, we focused our attention only on the films formed from solutions containing 0.3 M NaCl, for which no indications about the existence of the primary films (electrostatic stabilization) have been found.

By definition, the *critical thickness* h_{cr} is the thickness of a film at the moment of its rupture or black-spot formation. This moment is clearly seen in the respective intensity versus time interferograms, from which h_{cr} is determined with the help of eq 4. The obtained values of h_{cr} are presented in Table 1 and Figure 5 for different film radii and SDS concentrations C_{SDS} . As mentioned above, each experimental value in Table 1 (and point in Figure 5) is an average for 15 films formed under the same conditions. The standard error of mean for the experimental

Table 1. Measured and Theoretically Predicted Critical Thicknesses h_{cr} for Various Film Radii and SDS Concentrations at 0.3 M NaCl

measured film radius R (μm)	measured h_{cr} (nm)	predicted h_{cr} (nm) ($\Pi_{\text{hb}} \neq 0$)	predicted h_{cr} (nm) ($\Pi_{\text{hb}} = 0$)
Films from Solutions of $0.5 \mu\text{M}$ SDS + 0.3 M NaCl			
62	28.61 ± 0.55	28.67	23.11
93	32.94 ± 0.51	33.17	25.97
116	35.72 ± 0.49	35.79	27.59
132	37.25 ± 0.49	37.37	28.57
155	39.53 ± 0.52	39.39	29.81
Films from Solutions of $1.0 \mu\text{M}$ SDS + 0.3 M NaCl			
62	27.79 ± 0.54	27.12	23.15
93	30.57 ± 0.54	31.28	26.01
116	33.51 ± 0.49	33.68	27.64
132	35.00 ± 0.52	35.14	28.62
155	37.04 ± 0.50	37.01	29.86
Films from Solutions of $10.0 \mu\text{M}$ SDS + 0.3 M NaCl			
62	24.37 ± 0.53	23.80	23.52
93	26.89 ± 0.45	26.82	26.44
116	28.36 ± 0.49	28.54	28.11
132	29.35 ± 0.50	29.57	29.10
155	30.57 ± 0.54	30.89	30.34

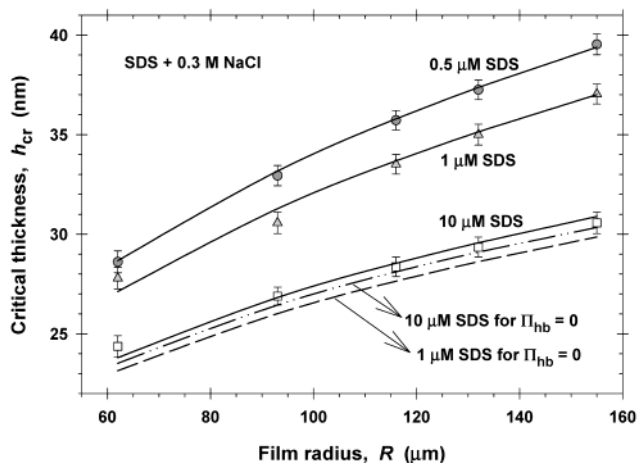


Figure 5. Plot of the critical thickness h_{cr} versus the film radius R at a 0.3 M fixed concentration of NaCl for three SDS concentrations, denoted in the figure (see Table 1). The theoretical curves are drawn with the help of the theory from section 3.2. The dashed and dash-dotted lines, for 1 and $10 \mu\text{M}$ SDS, respectively, are computed assuming an absence of the hydrophobic attraction, $\Pi_{\text{hb}} = 0$ (no adjustable parameters). The solid lines are fits of the experimental points for $\Pi_{\text{hb}} \neq 0$ (see eq 3), where B and λ are determined as adjustable parameters. $B = 0.656, 0.471,$ and $0.0334 \mu\text{J}/\text{m}^2$ for $0.5, 1,$ and $10 \mu\text{M}$ SDS, respectively, whereas $\lambda (=15.8 \text{ nm})$ is the same for the three lines.

points is also shown. The theoretical values in Table 1 (and the curves in Figure 5) are computed with the help of the theory described in section 3 for the two cases $\Pi_{\text{hb}} \neq 0$ and $\Pi_{\text{hb}} = 0$, which is with and without taking into account the action of the hypothetical hydrophobic surface force. The comparison of the theory and experiment is discussed in section 4.

3. Theoretical Background

3.1. Gibbs Elasticity and Mobility of the Film Surfaces. Let us first characterize the hydrodynamic regime of drainage of the investigated liquid films. The velocity of thinning $V = -dh/dt$ of a plane-parallel foam film is described by the expression^{41,42}

(41) Radoev, B. P.; Dimitrov, D. S.; Ivanov, I. B. *Colloid Polym. Sci.* **1974**, *252*, 50.

(42) Ivanov, I. B.; Dimitrov, D. S.; Radoev, B. P. *J. Colloid Interface Sci.* **1978**, *63*, 166.

(40) Kralchevsky, P. A.; Nagayama, K. *Particles at Fluid Interfaces and Membranes*; Elsevier: Amsterdam, 2001; Chapter 5.

$$\frac{V}{V_{\text{Re}}} = 1 + b + \frac{h_s}{h} \quad (6)$$

where V_{Re} , called the Reynolds velocity, is the rate of thinning of a liquid film sandwiched between two tangentially immobile surfaces and the last two terms in eq 6 express the contribution of the surface mobility:

$$b = \frac{3\eta D}{E_G h_a} \quad h_s = \frac{6\eta D_s}{k_B T \Gamma_1} \quad (7)$$

Here, η is the viscosity of the liquid, D and D_s are coefficients of the bulk and surface diffusion of the surfactant molecules, respectively, Γ_1 is the surfactant adsorption at the film surfaces, $E_G [= -\Gamma_1 (\partial\sigma/\partial\Gamma_1)]$ is the surface dilatational (Gibbs) elasticity, $h_a (= \partial\Gamma_1/\partial c_1)$ is the so-called adsorption length, with c_1 being the surfactant concentration, k_B is the Boltzmann constant, and T is the temperature.

To quantify the contribution of the surface mobility, we have to estimate the quantities b and h_s given by eq 7. With this end in view, we used a computer program, developed in ref 43, that allows one to calculate properties of the SDS adsorption monolayers at various surfactant and salt concentrations. This program is based on the theoretical fit of the SDS surface-tension isotherms for 11 different NaCl concentrations, by means of the van der Waals surface equation of state. The effects of the counterion binding and ionic activity coefficients are taken into account. In Table 2, we list the calculated SDS adsorption Γ_1 , adsorption (binding) of the Na^+ counterions at the headgroups in the SDS adsorption monolayer Γ_2 , Gibbs elasticity E_G , adsorption length h_a , and parameters b and h_s .

The data in Table 2 show that $b \ll 1$, and, hence, the effect of the bulk diffusion of SDS is completely negligible. In addition, for the data in Tables 1 and 2, we have $0.019 \leq h/h_s \leq 0.164$. To check whether the effect of h_s on the critical thickness h_{cr} is negligible, we calculated h_{cr} using the full hydrodynamic theory from ref 8, where all effects of the surface mobility are taken into account. The results obtained using, alternatively, the h_s values from Table 2 and setting formally $h_s = 0$ were coincident. For this reason, to process the data in Table 1, one can apply the simpler version of the theory for the case of the tangentially immobile film surfaces ($b = 0$, $h_s = 0$).

The conclusion that we can apply the theory for the tangentially immobile film surfaces is counterintuitive and calls for some discussion. Indeed, our experiments are carried out at low surfactant concentrations, and the surface density Γ_1 of the adsorbed surfactant molecules is also relatively low (see Table 2). Nevertheless, the dilatational elasticity E_G turns out to be large enough to suppress the *isotropic* (radial) modes of surface deformation (expansion-compression) during the thinning and to make the last two terms in eq 6 negligible (see the values of b and h_s in Table 2). In our analysis of the fluctuation capillary waves (the next section), we also consider waves of *radial* symmetry, which are expected to be of higher amplitude and the most "dangerous" for the film survival. The theoretical estimates show that the terms b and h_s can be neglected again. On the other hand, the dilatational elasticity E_G does not oppose two-dimensional *shear* flows, and in this respect, the film surfaces are mobile, as one intuitively anticipates. For

Table 2. Calculated Properties of SDS Monolayers at the Air–Water Interface with 0.3 M NaCl (Approach from Reference 43)

C_{SDS} (μM)	Γ_1 ($\mu\text{mol}/\text{m}^2$)	Γ_2 ($\mu\text{mol}/\text{m}^2$)	E_G (mN/m)	h_a (mm)	b	h_s (nm)
0.5	0.232	0.057	0.560	0.359	6.73×10^{-6}	4.68
1.0	0.385	0.115	0.921	0.270	5.44×10^{-6}	1.27
10.0	1.85	1.08	6.15	0.110	2.00×10^{-6}	0.586

this reason, when characterizing the film behavior upon drainage, it is better to term the surfaces "tangentially incompressible", instead of "tangentially immobile".

3.2. Theoretical Expressions for the Critical Thickness. As already mentioned, to form a foam film in the capillary cell (Figure 3), one has to apply a certain sucking capillary pressure P_c . As a result, the film thickness h gradually decreases because of the drainage of liquid. When h becomes sufficiently small, the attractive surface forces operative in the film (i.e., $\Pi_{\text{vw}} + \Pi_{\text{hb}}$) begin to influence the capillary waves on the film surfaces and to enhance their amplitude (Figure 1). The film continues to thin, and the waves continue to grow, until finally, at $h = h_{\text{cr}}$, the film surfaces locally touch each other, and either the film breaks or a black spot appears.

To mathematically describe this process, taking into account the axial symmetry of the cell in Figure 3, the shape of the corrugated film surfaces is presented as a superposition of Fourier–Bessel modes, proportional to $J_0(kr/R)$, for all possible values of the dimensionless wavenumber k (J_0 is the zeroth-order Bessel function).⁸ The mode, which has the greatest amplitude at the moment of film breakage and which causes the breakage itself, is called the critical mode, and its wavenumber is denoted by k_{cr} . The stability–instability transition for this critical mode happens at an earlier stage of the film evolution, when the film thickness is equal to h_{tr} , the so-called transitional thickness ($h_{\text{tr}} > h_{\text{cr}}$).^{4–8} The theory provides a system of three equations for determining the three unknown parameters h_{cr} , k_{cr} , and h_{tr} . According to ref 8, where the most complete theoretical description of the process of simultaneous film drainage and perturbation growth is given, the equations for determining h_{cr} , k_{cr} , and h_{tr} are

$$\frac{k_{\text{cr}}^2 \sigma}{R^2 h_{\text{cr}}^3} \int_{h_{\text{cr}}}^{h_{\text{tr}}} \frac{h^6}{P_c - \Pi} dh = \int_{h_{\text{cr}}}^{h_{\text{tr}}} \frac{h^3 \Pi'}{P_c - \Pi} dh \quad (8)$$

$$\Pi'(h_{\text{tr}}) = \frac{24 h_{\text{cr}}^3}{h_{\text{tr}}^4} [P_c - \Pi(h_{\text{tr}})] + \frac{\sigma h_{\text{tr}}^3 k_{\text{cr}}^2}{2 R^2 h_{\text{cr}}^3} \quad (9)$$

$$h_{\text{cr}} = \left(\frac{\sigma h_{\text{tr}}^2}{k_B T} \right)^{1/4} h_{\text{tr}} \exp \left(- \frac{k_{\text{cr}}^2}{32 h_{\text{cr}}^3} \int_{h_{\text{cr}}}^{h_{\text{tr}}} \frac{h^3 \Pi'}{P_c - \Pi} dh \right) \quad (10)$$

where, as before, $\Pi(h)$ is the disjoining pressure of the film, $\Pi' \equiv \partial\Pi/\partial h$. Equations 8–10 are corollaries (for the special case of tangentially incompressible film surfaces) from expressions derived in ref 8. In particular, eqs 8 and 9 follow from eqs 33 and 34 in ref 8, respectively, whereas eq 10 can be deduced from eqs 33 and 35 in ref 8. The principles of the numerical procedure for solving eqs 8–10 are outlined in section 3.4.

3.3. Expression for the Disjoining Pressure $\Pi(h)$. For the dependence $\Pi(h)$, we used eqs 2 and 3, where the van der Waals disjoining pressure Π_{vw} was calculated from the equation¹⁸

(43) Kolev, V. L.; Danov, K. D.; Kralchevsky, P. A.; Broze, G.; Mehreteab, A. *Langmuir* **2002**, *18*, 9106.

$$\Pi_{\text{vw}}(h) = -\frac{A(h)}{6\pi h^3} \quad (11)$$

The Hamaker parameter A depends on the film thickness h because of the electromagnetic retardation effect. $A(h)$ was calculated by means of a convenient expression derived by Russel et al.⁴⁴

$$A(h) = \frac{3h_p\nu_e}{4\pi} \frac{(n_i^2 - n_j^2)^2}{(n_i^2 + n_j^2)^{3/2}} \int_0^\infty \frac{(1 + 2\tilde{h}z) \exp(-2\tilde{h}z)}{(1 + 2z^2)^2} dz \quad (12)$$

Here, h_p ($=6.63 \times 10^{-34}$ J·s) is the Planck constant, ν_e ($\approx 3.0 \times 10^{15}$ Hz) is the main electronic absorption frequency, n_i and n_j are the refractive indexes of the outer phase (air, $n_i = 1$) and inner phase (aqueous solution, $n_j \approx 1.33$), respectively, dimensionless thickness \tilde{h} is defined by the expression $\tilde{h} = 2\pi\nu_e h n_j (n_i^2 + n_j^2)^{1/2} / c_0$, where c_0 ($=3.0 \times 10^8$ m/s) is the speed of light in a vacuum, and z is an integration variable. The “zero-frequency” contribution to $A(h)$ is negligible; it is screened owing to the high electrolyte concentration of 0.3 M NaCl (see, e.g., refs 18 and 44).

It should be noted that eq 4, which is currently used in foam film studies,^{9,10,37,38} gives the so-called “equivalent water thickness” h of the film. In other words, the real film, consisting of the aqueous core and two adjacent surfactant adsorption layers, is approximately treated as a uniform water layer of thickness h . Correspondingly, the refractive index of water is substituted for n in eq 4. For this reason, it is self-consistent to use $A(h)$ for water in eqs 11 and 12, which are employed to interpret the data. In our case, the surfactant adsorption is relatively low (Table 2), and we can expect that the experimental “equivalent water thickness” h , determined from eq 4, is very close to the real thickness of the film aqueous core.

As already mentioned, for $\Pi_{\text{hb}}(h)$, we used eq 3 from a paper by Eriksson et al.,¹⁷ which was found to provide a good fit of the data (see Figure 5). We also tried a simple exponential dependence, that is, $\Pi_{\text{hb}} \propto \exp(-h/\lambda)$; however, the obtained fit was not satisfactory. The fact that the hydrophobic surface force does not obey a simple exponential dependence has also been found by other authors who used an empirical superposition of two exponential functions.^{15,23}

3.4. Principles of the Numerical Procedure.

1. The input parameters are the experimental points (R, h_{cr}) in Table 1 and Figure 5 for the three different surfactant concentrations, the surface tension σ of the respective solutions, the refractive indices n_i and n_j in eq 12, the temperature $T = 25$ °C, and some known physical constants (k_B , h_p , c_0 , ν_e). The capillary pressure P_c is calculated from eq 5.

2. We give some tentative values to the parameters B and λ in eq 3.

3. An upper limit for the critical thickness h_{cr} is provided by the so-called stability thickness h_{st} , which is determined by numerically solving the equation $F(h_{\text{st}}) = 0$, where⁸

$$F(h_{\text{st}}) = 1 - \frac{h_{\text{st}} R^2 [\Pi'(h_{\text{st}})]^2}{48\sigma [P_c - \Pi(h_{\text{st}})]} \quad (13)$$

$F(h_{\text{st}})$ is a monotonic function; the single root for h_{st} is calculated using the bisection method. The root was searched within the range $0 < h_{\text{st}} < 1000$ nm. Here and

hereafter, $\Pi(h)$ and $\Pi'(h)$ are calculated by means of eqs 2, 3, 11, and 12.

4. We chose a tentative value of h_{cr} within the interval $0 < h_{\text{cr}} < h_{\text{st}}$.

5. We chose a tentative value of h_{tr} within the interval $h_{\text{cr}} < h_{\text{tr}} < h_{\text{st}}$. For the given h_{tr} and h_{cr} , the integrals in eq 8 are computed numerically, and k_{cr} is determined. Next, for the given h_{cr} , we determine h_{tr} by numerically solving the equation $G(h_{\text{tr}}) = 0$, an equivalent form of eq 9, where

$$G(h_{\text{tr}}) = 1 + \frac{h_{\text{tr}}^4 [\sigma h_{\text{tr}}^3 k_{\text{cr}}^2 - 2R^2 h_{\text{cr}}^3 \Pi'(h_{\text{tr}})]}{48h_{\text{cr}}^6 R^2 [P_c - \Pi(h_{\text{tr}})]} \quad (14)$$

$G(h_{\text{st}})$ is a monotonic function; the single root for h_{tr} is calculated using the bisection method.

6. We determine h_{cr} by numerically solving the equation $H(h_{\text{cr}}) = 0$, an equivalent form of eq 10, where

$$H(h_{\text{cr}}) = 1 - \frac{h_{\text{tr}} (\sigma h_{\text{tr}}^2)^{1/4}}{h_{\text{cr}} (k_B T)} \exp\left(-\frac{k_{\text{cr}}^2}{32h_{\text{cr}}^3} \int_{h_{\text{cr}}}^{h_{\text{tr}}} \frac{h^3 \Pi'}{P_c - \Pi} dh\right) \quad (15)$$

$H(h_{\text{cr}})$ is a monotonic function; the single root for h_{cr} is calculated using the bisection method. Thus, we determine the theoretical dependence $h_{\text{cr}} = h_{\text{cr}}^{(\text{th})}(R, B, \lambda)$. Formally setting $B = 0$, we obtain the theoretical predictions without hydrophobic interaction (see the last column of Table 1).

7. For each fixed SDS concentration, we determine preliminary values of the adjustable parameters B and λ by means of the least-squares method, i.e., by numerical minimization of the function

$$\Psi_i(B_i, \lambda_i) = \sum_{m=1}^{N_i} [h_{\text{cr}}^{(m)}(R^{(m)}, B_i, \lambda_i)]^2 \quad (16)$$

where $h_{\text{cr}}^{(m)}$ is the experimental value of h_{cr} , corresponding to a film radius $R^{(m)}$, the summation in eq 16 is carried out over all experimental points $[R^{(m)}, h_{\text{cr}}^{(m)}]$ corresponding to a given SDS concentration, denoted by the subscript i (see Figure 5), and N_i is the number of experimental points for the respective SDS concentration C_{SDS} . In this way, for the three fixed values of C_{SDS} in Table 1, we determine three preliminary couples of parameter values (B_1, λ_1) , (B_2, λ_2) , and (B_3, λ_3) . We use the obtained values B_1 , B_2 , B_3 , and $\lambda = (\lambda_1 + \lambda_2 + \lambda_3)/3$ as an initial approximation to start the four-parameter minimization procedure in the next point.

8. We determine the final values of the four adjustable parameters B_1 , B_2 , B_3 , and λ using again the least-squares method applied to the whole set of experimental points, by numerical minimization of the function

$$\Psi(B_1, B_2, B_3, \lambda) = \sum_{i=1}^3 \Psi_i(B_i, \lambda) \quad (17)$$

where Ψ_i is given by eq 16.

4. Comparison of the Theory and Experiment

4.1. Results from the Fits and Discussion. Using the procedure from section 3.4, we processed the data points in Figure 5 and determined (as adjustable parameters) B and λ , which characterize the hydrophobic interaction (see eq 3). Because B characterizes the interfacial hydrophobicity, while λ is a bulk property

(44) Russel, W. B.; Saville, D. A.; Schowalter, W. R. *Colloidal Dispersions*; Cambridge University Press: New York, 1989.

Table 3. Parameters in Equation 3 for Foam Films (Table 1) and Hydrophobized Mica (Reference 17)

system	λ (nm)	B (mJ/m ²)	std dev (nm)
0.5 μ M SDS + 0.3 M NaCl	15.8	6.56×10^{-4}	0.141
1.0 μ M SDS + 0.3 M NaCl	15.8	4.71×10^{-4}	0.475
10 μ M SDS + 0.3 M NaCl	15.8	3.34×10^{-5}	0.355
DDOA-covered mica ¹⁷	15.8	0.6	
F-surfactant-covered mica ¹⁷	15.8	0.9	

related to the propagating hydrogen bonding of the water molecules, from the fit of the data, we obtain three different values of B (denoted by B_1 , B_2 , and B_3) for the three experimental SDS concentrations and a single value of λ , the same for the whole set of data. Note that the SDS concentrations used are extremely small and could hardly affect the hydrogen bonding in the bulk (and the value of λ), while the adsorption of SDS is material and can affect the interfacial hydrophobicity (and the value of B). The results are listed in Table 3 where, for comparison, the values of λ and B , determined in ref 17 for the hydrophobized solid surfaces immersed in water, are also given.

The last column in Table 3 shows the standard deviation of the fits of the data for $h_{cr}(R)$ (the three solid lines in Figure 5). It is seen that the theory compares very well with the experimental points. Moreover, the determined decay length of the hydrophobic force in foam films ($\lambda = 15.8$ nm) practically coincides with the value of λ obtained in ref 17 for mica covered with the hydrocarbon monolayer (DDOA = dimethyldioctadecylammonium bromide) and a monolayer from the fluorinated cationic surfactant. It should be noted that the function $\Psi(B_1, B_2, B_3, \lambda)$ in eq 17 has a sharp minimum with respect to all of its four arguments.

The last column in Table 1 and the lower two curves in Figure 5 are calculated by substituting $B = 0$, which means that the hydrophobic surface force is set to zero ($\Pi_{hb} = 0$) (see eq 3). In this case, all of the parameters of the theory are known, and the theoretical curves are drawn without using any adjustable parameters. In Figure 5, the respective computed curve for 1 μ M SDS practically coincides with that for 0.5 μ M SDS; for this reason, the latter curve is not shown in the figure. The curves calculated for $\Pi_{hb} = 0$ lie far away from the experimental points for 0.5 and 1 μ M SDS; this fact can be interpreted as a consequence of the action of the hydrophobic force in the film. Note also that $h_{cr}(10 \mu\text{M SDS}) > h_{cr}(1 \mu\text{M SDS})$ for the calculated curves assuming $\Pi_{hb} = 0$, whereas exactly the opposite tendency holds for the respective experimental points in Figure 5.

From the data in Table 1 and Figure 5, one may conclude that the van der Waals interaction, alone, is insufficient to explain the measured critical thickness of foam films h_{cr} especially for the lower SDS concentrations of 0.5 and 1 μ M. If the effect is attributed to the hydrophobic attraction expressed by eq 3, then a very good agreement between the theory and experiment can be achieved (Figure 5). The obtained values of B decrease with the rise of C_{SDS} (see Table 3). This is a reasonable result insofar because the film surfaces become more and more hydrophilic with the increase of C_{SDS} and, correspondingly, with the rise of the SDS adsorption Γ_1 . The dependence $B(\Gamma_1)$ is discussed in the next subsection.

Finally, it should be noted that the obtained values of B for foam films are much less than those for the hydrophobized mica (Table 3). This means that the air-water interface is much less hydrophobic than the hydrophobized mica.

4.2. Dependence of B on the Ionic Adsorption. We checked the correlation of the obtained values of B (Table

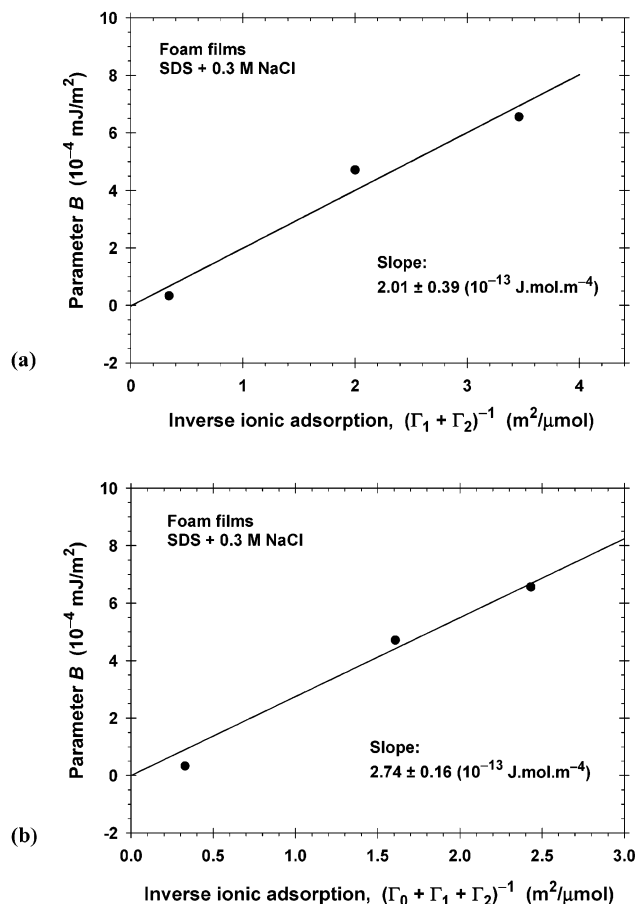


Figure 6. Plot of the parameter B , which characterizes the interfacial hydrophobicity, versus the inverse adsorption of ions at the air-water interface. (a) Plot of B versus $(\Gamma_1 + \Gamma_2)^{-1}$. (b) Plot of B versus $(\Gamma_0 + \Gamma_1 + \Gamma_2)^{-1}$. Γ_0 , Γ_1 , and Γ_2 are the adsorptions of the OH^- , DS^- , and Na^+ ions, respectively.

3) with the properties of the surfactant monolayers listed in Table 2. We found that the data for B , plotted versus $(\Gamma_1 + \Gamma_2)^{-1}$, comply with a linear regression, which has a zero intercept (see Figure 6a). This result seems reasonable, because when C_{SDS} increases and we have $(\Gamma_1 + \Gamma_2)^{-1} \rightarrow 0$, the air-water interface becomes more hydrophilic, which implies $B \rightarrow 0$. Indeed, as discussed earlier, from the fit of the data in Figure 2, it follows that, at $C_{SDS} = 0.43$ mM, we already have $B = 0$. In other words, one could regard dodecyl sulfate (DS^-) and the Na^+ ions as hydrophilic, and, consequently, their adsorption should hydrophilize the air-water interface.

The empirical dependence $B \propto (\Gamma_1 + \Gamma_2)^{-1}$ can be considered as an asymptotic expression, which is valid for high adsorptions, $(\Gamma_1 + \Gamma_2) \rightarrow \infty$. Obviously, this empirical dependence is not valid in the other asymptotic limits, $(\Gamma_1 + \Gamma_2) \rightarrow 0$, where it gives $B \rightarrow \infty$, which is a physically irrelevant result. A more versatile empirical expression for B can be obtained if we recall that even the surface of pure water (without any dissolved SDS or NaCl) bears a negative background surface charge. This electric charge is pH-dependent, and it is believed to be due to the adsorption of the hydroxyl (OH^-) ions at the air-water interface.⁴⁵⁻⁵⁰ Correspondingly, we could seek B in the

(45) Mctaggart, H. A. *Philos. Mag.* **1914**, 27, 29.

(46) Alty, T. *Proc. R. Soc. London, Ser. A* **1924**, 106, 315.

(47) Usui, S.; Sasaki, H.; Matsukawa, H. *J. Colloid Interface Sci.* **1981**, 81, 80.

(48) Yoon, R.-H.; Yordan, J. L. *J. Colloid Interface Sci.* **1986**, 113, 430.

form

$$B = \frac{K}{\Gamma_0 + \Gamma_1 + \Gamma_2} \quad (18)$$

where K is an empirical constant and Γ_0 is the adsorption of the OH^- ions. The fit of the data with eq 18, which is shown in Figure 6b, corresponds to $K = 2.74 \times 10^{-13} \text{ J}\cdot\text{mol}\cdot\text{m}^{-4}$ and $\Gamma_0 = 0.122 \mu\text{mol}\cdot\text{m}^{-2}$. The maximum value of B , predicted by eq 18 for a water phase without SDS, that is, for $(\Gamma_1 + \Gamma_2) \rightarrow 0$, is $B_{\text{max}} = K/\Gamma_0 = 22.5 \times 10^{-4} \text{ mJ/m}^2$. To obtain more reliable values of Γ_0 and B_{max} , with processing of a set of more experimental points, additional measurements at lower SDS concentrations should be carried out.

As discussed above, the presence of the adsorbed SDS molecules renders the air–water interface more hydrophilic. This effect is due to the surfactant headgroups. On the other hand, in dilute SDS monolayers, where the molecules are well spaced, it is thought that the alkyl chains lie flat on the water surface. This could mean that some of the “hydrophobic surface” is due to the hydrocarbon–water contact. However, the observed influence of SDS on the behavior of the film implies that the “hydrophilizing” effect of the surfactant headgroup prevails over the “hydrophobizing” effect of the alkyl chains.

5. Summary and Conclusions

At sufficiently high electrolyte concentrations (at suppressed electrostatic repulsion), the foam films gradually

(49) Graciaa, A.; Morel, G.; Saulnier, P.; Lachaise, J.; Schechter, R. S. *J. Colloid Interface Sci.* **1995**, *172*, 131.

(50) Marinova, K. G.; Alargova, R. G.; Denkov, N. D.; Velev, O. D.; Petsev, D. N.; Ivanov, I. B.; Borwankar, R. P. *Langmuir* **1996**, *12*, 2045.

thin, until reaching a certain critical thickness, and then they break. The value of this critical thickness is sensitive to the magnitude of the attractive surface forces acting in the film. We experimentally investigated the breakage of the films formed from aqueous solutions of SDS in the presence of 0.3 M NaCl added. The theoretical fits of the obtained data for the critical thickness (Table 1 and Figure 5) indicate that the van der Waals interaction, alone, is insufficient to explain the results, especially for the lower SDS concentrations of 0.5 and 1 μM . If the difference is attributed to the hydrophobic attraction (eq 3), then a very good agreement between the theory and experiment is achieved (Figure 5). From the best fit, we determine the decay length of the hydrophobic force to be $\lambda \approx 15.8 \text{ nm}$, which coincides with the value obtained by other authors for the hydrophobized mica surfaces¹⁷ (see Table 3). The strength of the hydrophobic interaction, characterized by the parameter B , increases with the decrease of the SDS concentration (Table 3), which can be explained with the fact that between the adsorbed surfactant molecules greater areas of bare hydrophobic air–water interface are uncovered. In the investigated concentration range, B is found to be inversely proportional to the surface density of the adsorbed ions (eq 18 and Figure 6). At higher SDS concentrations, the hydrophobic interaction in foam films is suppressed, in agreement with the previous results (Figure 2).

Acknowledgment. This work was supported by Unilever Research U.S. The authors are indebted to Prof. Ivan B. Ivanov for the stimulating discussions.

LA0357514